Efficient Convergent Energy Transfer in a Stereoisomerically Pure Heptanuclear Luminescent Terpyridine-Based Ru(II)-Os(II) Dendrimer

Simon Cerfontaine,[†] Quentin Duez,[⊥,£] Ludovic Troian-Gautier,[‡] Gabriella Barozzino-Consiglio,[†] Frédérique Loiseau,[Γ] Jérôme Cornil,[£] Julien De Winter,[⊥] Pascal Gerbaux[⊥] and Benjamin Elias[†*]

[†] Université catholique de Louvain (UCLouvain), Institut de la Matière Condensée et des Nanosciences (IMCN), Molecular Chemistry, Materials and Catalysis (MOST), Place Louis Pasteur 1, bte L4.01.02, 1348 Louvain-la-Neuve, Belgium.

[⊥] Organic Synthesis and Mass Spectrometry Laboratory, University of Mons - UMONS, 23 Place du Parc, B-7000 Mons, Belgium.

[£] Laboratory for Chemistry of Novel Materials, Center of Innovation and Research in Materials and Polymers (CIRMAP) – University of Mons (UMONS), Place du Parc 23, B-7000 Mons, Belgium.

[‡] Laboratoire de Chimie Organique, Université libre de Bruxelles (ULB), CP 160/06, 50 avenue F.D. Roosevelt, 1050 Brussels, Belgium.

[Γ] Univ. Grenoble Alpes, CNRS, DCM, 38000 Grenoble, France.

Abstract

The stereoisomerically pure synthesis of a novel heptanuclear Ru(II)-Os(II) antenna bearing multitopic terpyridine ligands is reported. An unambiguous structural characterization was obtained by ^{1}H NMR spectroscopy and ion mobility spectrometry (IMS-MS). The heptanuclear complex exhibits large molar absorption coefficients (77,900 $M^{-1}cm^{-1}$ at 497 nm) and undergoes unitary, downhill, convergent energy transfer from the peripheral Ru(II) subunits to the central Os(II) that displays photoluminescence with a lifetime (τ =161ns) competent for diffusional excited-state electron transfer reactivity in solution.

Introduction

The development of photoluminescent and redox active dendrimers represents an active, challenging subject of research. Dendrimers are prime candidates for artificial light-harvesting antennae due to their ability to funnel energy to a desired location through a cascade of energy transfer processes upon absorption by well-positioned chromophores.[1, 2] The final energy acceptor can then undergo excited-state electron transfer with relevant catalysts or molecules.[3] The interest in these dendrimers has been revived by their ability to perform useful transformations relevant for solar fuel production[4-11] and catalysis.[12, 13] The antenna effect can only be achieved in metal-based dendrimers with suitably organized subunits, in terms of energy, position and deactivation rate constants.[14] For dendrimers with equivalent peripheral metal centers connected to a central metal unit, an antenna effect is obtained if a convergent downhill energy transfer occurs.[15] This implies favorable driving force between the energy donor and acceptor moieties.[16, 17] Such favorable energy transfers are commonly observed between Ru(II) and Os(II) polypyridyl complexes.[14, 18-22] The use of Ru(II) peripheral subunits connected to an Os(II) central unit by suitable bridging ligands[23, 24] that allow for fast and efficient converging energy transfer, qualifies these dendrimers as efficient molecular antennae.[25-28] However, although attractive targets, dendrimer design remains challenging. Increased light absorption can be achieved by introducing intermediate metal subunits between the peripheral Ru(II) and central Os(II) and thereby increasing the nuclearity of the dendrimer. However, crucially, the thermodynamics of the intermediate metal units must be in-between those of the peripheral Ru(II) subunits and the Os(II) center, or the convergent energy transfer becomes inefficient or inoperative.[29, 30] Furthermore, most Ru(II)-Os(II) polynuclear complexes reported to date were obtained using bidentate ligands that, unless stereospecific synthetic approaches are used, do not allow for stereo (Λ and Δ) and geometric (*mer* and *fac*) control.[31-34] Hence, mixtures of several diastereoisomers resulted, complicating structural characterization and, in some rare case, impacting the excited-state properties[34-36] and vectorial energy transfer, or interaction with chiral molecules.[37-42]

Complexes with tridentate ligands, such as 2,2':6',2''-terpyridine (tpy), do not yield such isomers and can produce well-characterized geometric patterns.[18, 43-45] In addition, tpy complexes typically exhibit enhanced stability due to the chelate effect, compared to bpy analogues. The use of tpy ligands was already reported for the synthesis of dendrimers.[46, 47] Unfortunately, tri- and pentanuclear Ru(II)-Os(II) complexes as previously reported by Constable *et al.* solely underwent energy transfer at low temperatures.[48]

Herein, the synthesis of a stereoisomerically pure heptanuclear dendrimer **3**, containing a central Os(II) core surrounded by six Ru(II) centers is reported (**Scheme 1**). An efficient convergent downhill energy transfer occurs from the four peripheral Ru(II), via the two intermediate Ru(II), to the central Os(II) energy acceptor. Dendrimer **3** was fully characterized by in depth ^{1}H NMR analysis and mass spectrometry in concert to ion mobility spectrometry coupled to mass spectrometry (IMS-MS). Finally, the redox and photophysical properties of **3** were also investigated.

Scheme 1. Synthesis pathway of dendrimer 3.

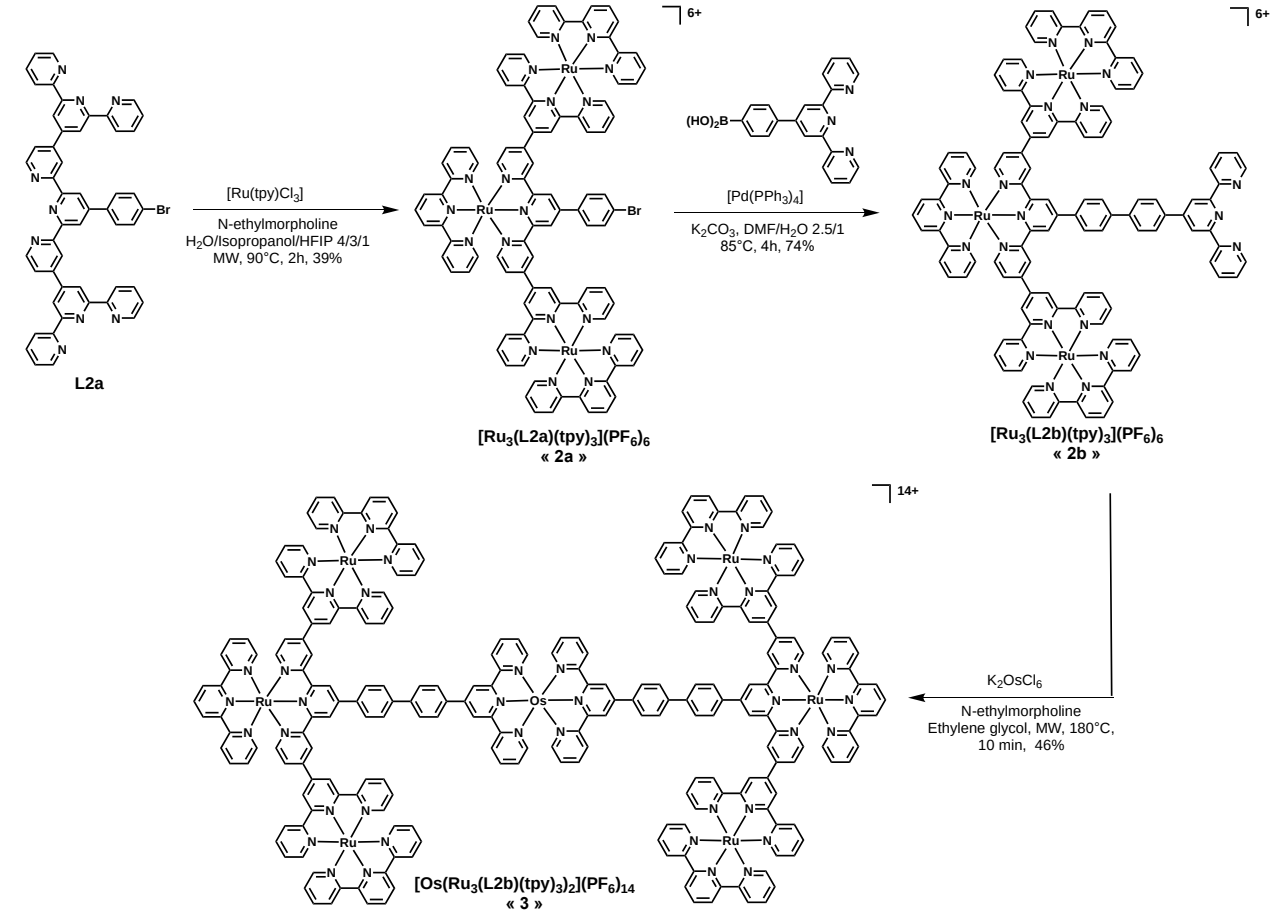

Results and Discussion

Dendrimer **3** was prepared by a three-step synthesis (**Scheme 1**). Firstly, complex **2a** was synthesized at 90°C under microwave irradiation by complexation of [Ru(tpy)Cl_3] with the brominated bridging ligand[49] in a water/isopropanol/hexafluoroisopropanol mixture in the presence of *N*-ethylmorpholine as reducing agent. Secondly, the additional tpy coordination site (**2b**) was generated by reacting **2a** with (4-([2,2':6',2''-terpyridin]-4'-yl)phenyl)boronic acid in the presence of Pd(0). Finally, the heptanuclear dendrimer **3** was obtained after reaction

between **2b** and K_2OsCl_6 in ethylene glycol at 180 °C under microwave irradiations. Complexes **1** and **2** were synthesized as previously described.[50]

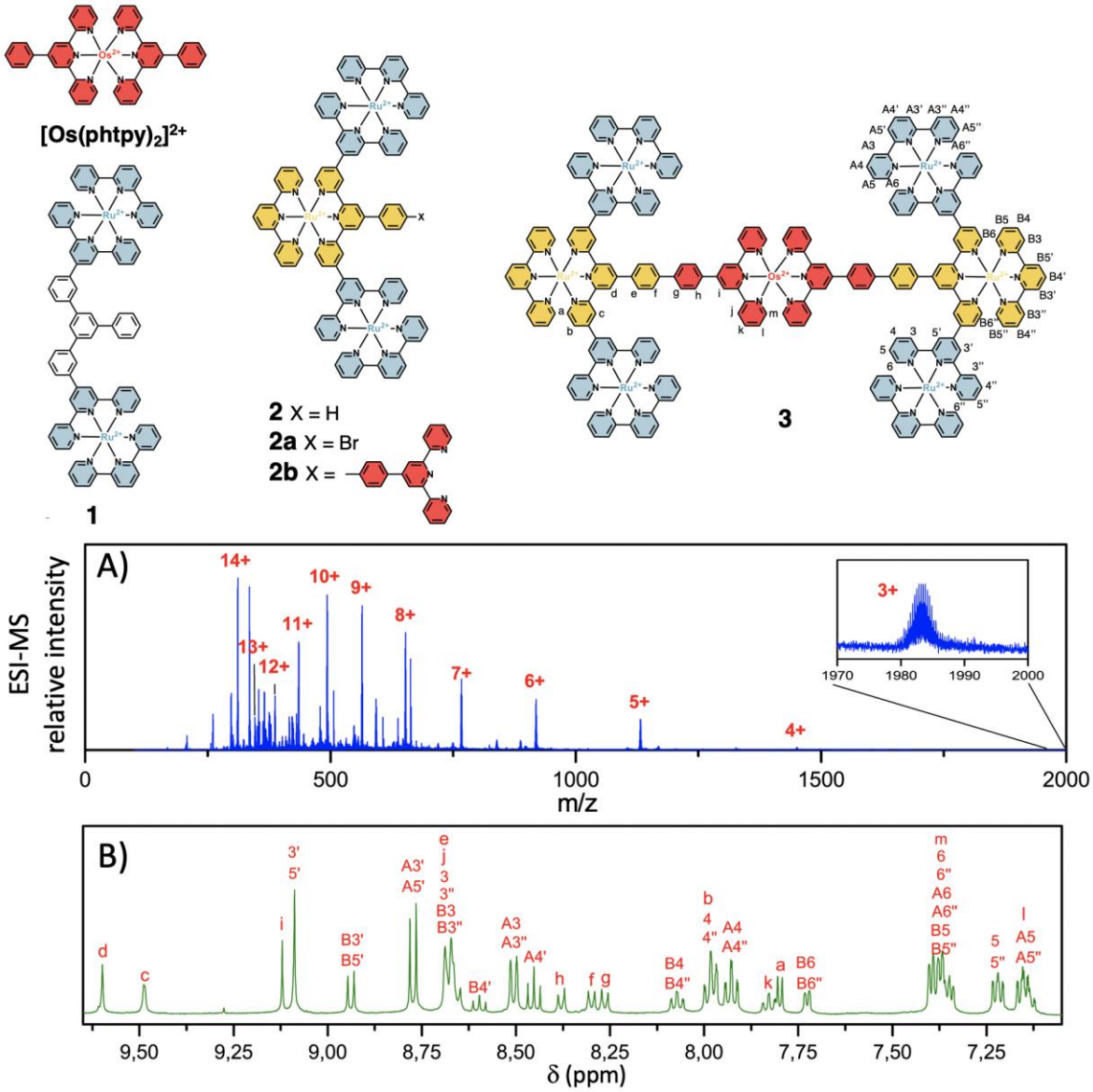

Figure 1. Structures of the polynuclear complexes **1-3** and $[Os(phtpy)_2]^{2+}$ (top). ESI-MS spectrum (a) with charged states assigned to all signals. ^{1}H NMR spectrum (b) of **3** with the corresponding peak assignment (NMR recorded in CD_3CN at 295K at 500 MHz).

Dendrimer **3** and its precursors were unambiguously characterized by HRMS measurements and ^{1}H NMR spectroscopy (**Figures 1a and S1-S33**). The use of terpyridine moieties resulted in a stereoisomerically pure dendrimer **3**. Consequently, the ^{1}H NMR spectrum (**Figure 1b**) was well-defined and could be fully assigned by combination of ^{1}H-^{1}H COSY and ^{1}H-^{1}H NOESY 2D experiments (**Figures S7-S17**). 2D DOSY NMR of **2b** and **3** confirmed that only pure compounds were present in solution (**Figures S18-S23**). The hydrodynamic volume of **3**

was determined by DOSY as 1.84 times larger than that of **2b** (**Tables S1-S3**). The ESI mass spectrum of **3** (positive mode -**Figure 1a**) featured a series of well-defined peaks corresponding to adducts of **3** with PF_6^- counterions, *i.e.* $[\mathbf{3} + n\ PF_6]^{(14-n)+}$ cations with charges that ranged from 3+ to 14+ (**Figures S29-S33**). Further information was obtained by ion mobility spectrometry (IMS-MS),[51] which is an experimental technique that separates ions based on their mobility in a cell filled with buffer gas (He or N_2) under an applied electric field. The drift time through the cell, *i.e.* the measured variable in IMS experiments, is directly proportional to the ion collision cross section (CCS), which represents the effective interaction area between the ion and the buffer gas and can be associated with the 3D structure.[51] Narrow and unimodal arrival time distributions (ATD) were measured for the highest charge state of **2b** (6+) and **3** (14+), which is indicative of unique species (**Figure S34**). Average experimental CCS values of 500 $Å^2$ and 981 $Å^2$ were determined for the highest charge states of **2b** and **3,** respectively. These agreed with the theoretically average values (493 $Å^2$ and 950 $Å^2$) predicted by Molecular Dynamics simulations (**Figure S35**). Understandably, the experimental CCS of **3** was almost twice that of **2b**, in agreement with DOSY experiments.

Cyclic and differential pulse voltammograms (DPV) of **3** are presented in **Figures 2a** and **2b**, while the corresponding electrochemical data are gathered in **Table 1**. Two reversible processes were recorded, the first at +0.91 V vs Ag/AgCl, followed by the second at +1.31 V vs Ag/AgCl. The first process was attributed to metal-centered $Os^{(III/II)}$ oxidation, consistent with the oxidation potential of $[Os(phtpy)_2]^{2+}$ (**Figures S36-S37**). The second process was attributed to the simultaneous one-electron $Ru^{(III/II)}$ oxidation of the six ruthenium centers of **3**.

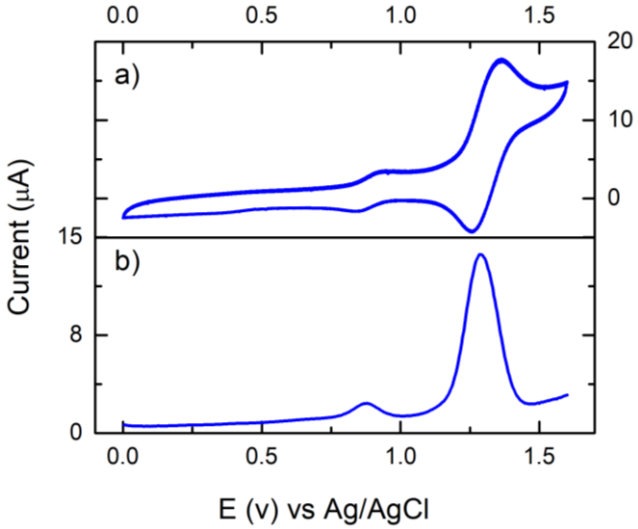

Figure 2. Cyclic (a) and differential pulse (b) voltammograms of **3** recorded in 0.1M [n-Bu_4][PF_6^-] acetonitrile electrolyte.

Table 1. Electrochemical data of the indicated complexes in 0.1M [n-Bu$_4$][PF$_6^-$] acetonitrile electrolyte at 293K.

Compound	$E_{1/2}^{ox}$	$E_{1/2}^{red}$
		(V vs Ag/AgCl)
1	+1.30	–1.19; –1.41
2	+1.37	–0.90; –0.96; –1.25, –1.38
3	+0.91; +1.31	–0.93; –0.99; –1.20; –1.40
[Os(phtpy)$_2$]$^{2+}$	+0.94	–1.15; –1.42

The oxidation of both peripheral and intermediate Ru(II) centers occurred at the same potential, as observed for **2**. Hence, limited electronic interaction was conferred by the bridging ligand connecting the Ru(II) centers. In DPV, the intensity of the Ru$^{(III/II)}$ oxidation wave was about six-fold that of the Os$^{(III/II)}$ oxidation, in agreement with the metallic composition of **3**. The ligand-centered reductions of **3** were assigned by comparison with the corresponding parent complexes (**Figure S38**). For compound **1**, which behaves similarly to [Ru(tpy)$_2$]$^{2+}$,[45] the first reduction wave (–1.19 V) was attributed to the reduction of two terpyridine moieties connected to two Ru(II) and the second reduction wave (–1.41 V) to the two remaining terpyridine moieties. The first (–0.90 V) and second (–0.96 V) reduction peaks of **2** were attributed to two successive one-electron reductions of the bridging ligand,[50] more precisely, the part connecting the different Ru(II) centers. The peak at –1.25 V was attributed to the reduction of one of the three terpyridine ligands connected to the Ru(II) centers and the peak at –1.38 V was attributed to the reduction of the last two terpyridine ligands connected to the Ru(II) centers. Finally, for **3** the first (–0.93 V) and second (–0.99 V) reduction peaks were attributed to two successive reductions of both bridging ligands, in a similar way as observed for **2**. The peak at –1.20 V was attributed to the reduction of two of the six terpyridine ligands connected to the Ru(II) centers and to one of the two terpyridine moieties connected to the Os(II), at similar potential than for [Os(phtpy)$_2$]$^{2+}$. The peak at –1.40 V was attributed to the reduction of the last four terpyridine ligands connected to the Ru(II) centers and the last terpyridine connected to the Os(II).

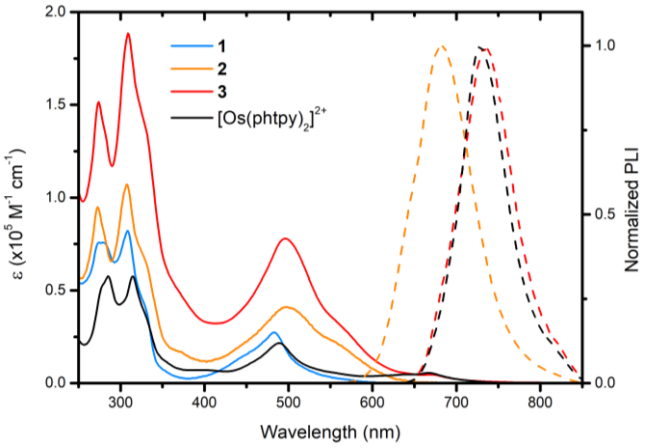

Figure 3. Absorption (solid) and photoluminescence (dash) spectra of the indicated complexes recorded in acetonitrile at 293K.

The absorption and photoluminescence (PL) spectra of the different compounds are shown in **Figure 3** and the corresponding photophysical data are gathered in **Table 2**. The absorption spectra are typical for Ru(II) and Os(II) polypyridyl complexes, with bands in the UV region attributed to ligand-centered transitions. The visible region is mostly dominated by metal-to-ligand charge transfer (MLCT) transitions in Ru(II) and Os(II) subunits. The band around 500 nm was attributed to spin-allowed ^{1}MLCT transitions for both metals, whereas the transition around 670 nm was assigned to the spin-forbidden ^{3}MLCT transition in Os(II) derivatives.[45] The absorption spectrum of **3** closely corresponded to the sum of the individual spectra of its constituent units, highlighting once again their limited electronic interaction in the ground state. For all complexes, the PL was typical for ^{3}MLCT excited-state. The very weak PL of **1** at 293 K (**Figure S39**) was a consequence of the very fast and efficient non-radiative deactivation through the triplet metal center (^{3}MC) excited-state.[45] The unusually long-lived PL of **2** arose from an energy transfer from the two peripheral Ru(II) to the intermediate Ru(II) center, which displayed significantly less non-radiative deactivation through the ^{3}MC excited-state.[50] The PL of **3** was characteristic of the Os(II) subunit, as confirmed by comparison with $[Os(phtpy)_2]^{2+}$. The absence of significant deactivation through the ^{3}MC at 293K in Os(II) terpyridine complexes led to longer excited-state lifetime and greater PL quantum yield (Φ_{PL}) compared to their Ru(II) counterparts.[52] In **3**, there was no residual photoluminescence of Ru(II) subunits, indicating that they were fully quenched by the Os(II) center.

Table 2 Spectroscopic and photophysical data for the indicated complexes

	Absorption[a]	**Photoluminescence**[a]				
	λ_{max} nm (ε, $M^{-1}cm^{-1}$)	λ_{max} (nm)[b]	Φ_{PL}[c]	ϕ (ns)[c]	I_{rel} (490 nm)[d, e]	I_{rel} (650 nm)[d, f]
1	483 (27,500)	639	[g]	[g]		
2	497 (41,000)	682	0.0018 (0.0014)	119 (101)		
3	497 (77,900); 670 (4600)	736	0.012 (0.0073)	161 (98)	60	57
$Os(phtpy)_2]^{2+}$	489 (21,600); 667 (5500)	728	0.020 (0.011)	184 (102)	100	100

[a] Acetonitrile solution, 293 K. [b] Excitation at λ_{max} of ^{1}MLCT. [c] In argon purged acetonitrile solution with values for air equilibrated solution in parenthesis. [d] Isoabsorptive solution of **3** and $[Os(phtpy)_2]^{2+}$ at the wavelength of excitation. [e] Relative intensity with λ_{exc} = 490 nm. At this excitation wavelength both the Ru and Os subunits are excited. [f] Relative intensity with λ_{exc} = 650 nm. At this excitation wavelength, only the Os subunit is excited. [g] Luminescence too weak to be quantified.

Isoabsorptive solution of **3** and $[Os(phtpy)_2]^{2+}$ were then excited at 650 nm or 490 nm (**Figure 4**). For **3**, at 490 nm, the Os(II) center absorbed approximatively $1/7^{th}$ of the light, whereas the remaining portion of light was absorbed by Ru(II) subunits. At 650 nm, both $[Os(phtpy)_2]^{2+}$ and the Os(II) in **3** were solely responsible for light absorption. In both cases, the Os(II) relative emission intensities were identical within the experimental error (**Table 2**). This indicated that in **3**, the energy absorbed by the Ru(II) subunits was quantitatively funneled to the Os(II) center.[18] This was also confirmed by the close match between the absorption and the excitation spectra (**Figure S41**).

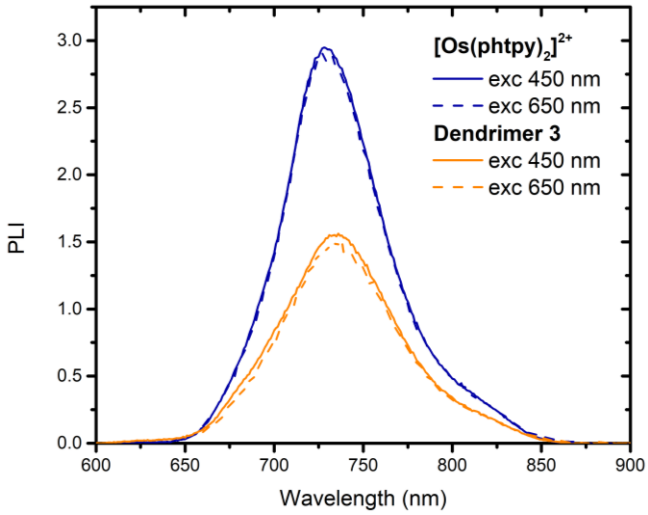

Figure 4. Emission spectra for $[Os(phtpy)_2]^{2+}$ and **3** in degassed acetonitrile solution at 293 K, a) excitation at 490 nm and b) excitation at 650 nm. The solutions are isoabsorptive at the wavelength of excitation.

The driving force for energy transfer (ΔG_{EnT}) between ^{3}MLCT excited-state from the peripheral Ru(II) to the intermediate Ru(II) was estimated to be –0.13 eV based on the PL maxima of **1**-**3** at 293 K. ΔG_{EnT} = – 0.14 eV was determined for energy transfer from the intermediate Ru(II) to the central Os(II). As a consequence, a unidirectional downhill convergent energy transfer with unitary efficiency was observed (**Figure 5**). This observation implied that the rate constants for energy transfer must largely exceed the intrinsic decay rate constants of individual subunits. Interestingly, the increased number of metal centers was accompanied by an increase of the excited-state lifetime and Φ_{PL} (**3**>**2**>**1**), concomitant with a decrease in the energy of the ^{3}MLCT excited-state. This underlines that the PL properties are mainly determined by the final energy acceptor in light-harvesting molecular antennae with efficient energy transfer.

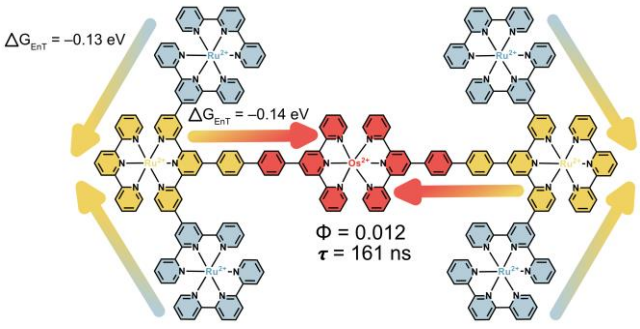

Figure 5. Schematic representation of the energy gradient in the light-harvesting dendrimer **3**.

Conclusions

In conclusion, we successfully synthesized and characterized a new stereoisomerically pure heptanuclear Ru(II)-Os(II) dendrimer templated by multitopic ligands with terpyridine binding site. Collision cross section values of 500 $Å^2$ and 981 $Å^2$ were determined by IMS-MS for the highest charge states of **2b** and **3**, respectively, which agreed with in depth DOSY measurements. The formation of dendrimer **3** was accompanied by a drastic increase in visible light absorption (ε = 77,900 $M^{-1}cm^{-1}$ at 497 nm). Within **3**, the energy stored from visible-light excitation was efficiently funneled from the four peripheral Ru(II) to the two intermediates Ru(II) and finally to the Os(II) center via energy transfer. This was made possible by the judicious design of **3** in which the energy of the corresponding ^{3}MLCT excited-states induced a convergent downhill energy transfer. As a consequence, **3** behaves as a light-harvesting molecular antenna with unitary energy transfer efficiency in which the final acceptor has an excited-state lifetime sufficiently long to perform diffusional excited-state electron transfer reactivity in solution.[53]

Experimental

Materials. Acetonitrile ≥ 99.9% (VWR), tetrahydrofuran ≥ 99.9% (VWR), diethyl ether ≥ 99% (VWR), isopropanol ≥ 99.9% (VWR), anhydrous acetonitrile ≥ 99.8% (Sigma-Aldrich), anhydrous *N,N*-dimethylformamide ≥ 99.8% (Sigma-Aldrich), ethylene glycol ≥ 99% (Roth), hexafluoisopropanol (HFIP) 99% (Fluorochem), $[NH_4][PF_6]$ 99% (Fluorochem), $[nBu_4][PF_6]$ 97% (Fluorochem), *N*-ethylmorpholine 99% (Sigma Aldrich), 2,2‘:6’,2’’-terpyridine 97 % (Alfa Aesar), 2,2’-bipyridine 98% (Fluorochem), triphenylphosphine 99% (Acros Organic), 2-acetylpyridine 98% (Acros Organic), benzaldehyde 98+% (Acros Organic), 4-formylphenylboronic acid 98% (Fluorochem), $RuCl_3.xH_2O$ 35-40% Ru (Acros Organic), $K_2OsCl_6.xH_2O$ ≥ 38.7% Os (Alfa Aesar), $PdCl_2$ 99% (Fluorochem), KNO_3 ≥ 99% (Roth), SiO_2 40-63 μm (Rocc), Sephadex LH-20 (GE Healthcare), 0.45 μm PTFE syringe filter (Rocc) were used as received. $[Ru(tpy)Cl_3]$,[54] $[Ru(bpy)_3](PF_6)_2$,[55] $[Os(bpy)_3](PF_6)_2$,[56] $[Os(phtpy)_2](PF_6)_2$,[44] $[Pd(PPh_3)_4]$,[57] 4'-phenyl-2,2':6',2''-terpyridine (phtpy)[58] and (4-([2,2':6',2''-terpyridin]-4'-yl)phenyl)boronic acid[59] were synthesized according to literature procedures. Water was purified with a Millipore Milli-Q system. The precipitates were isolated by centrifugation at 6000 rpm for five minutes in a Hettich Universal 320 centrifuge.

Microwave synthesis. Microwave (MW) syntheses were performed on a Milestone MicroSYNTH labstation under magnetic stirring. Typically, the conditions allowed the vessels

to reach the desired temperature in 5 minutes and the vessels were held at the desired temperature for the indicated period of time.

Nuclear Magnetic Resonance. All NMR spectra were recorded at room temperature (295 K) on a Bruker Avance 500 spectrometer using a BBO{^{1}H,X} probehead with a *z*-gradient. Calibrations were made using residual solvent peak as internal standard (for ^{1}H, δ = 1.94 ppm in CD_3CN). NMR spectra were processed using MNOVA software. Chemical shifs (δ) are given in parts per million (ppm) and the coupling constants (*J*) in hertz (Hz). The following abbreviations were used to designate the multiplicities: s = singlet, d = doublet, t = triplet and m = multiplet. Standard zg programs were employed for ^{1}H NMR experiments. Relaxation delay (d1) was 10 s and the number of scans were from 16 to 256. ^{1}H,^{1}H-COSY spectrum was acquired with 4096 data points in f2 and with 300 increments in f1, using 24 scans for each FID. The recycling delay was 2.0 s; acquisition mode was DQD; one time zero filling in f1; pure sine bell window function in f1 dimension and π/2 shifted sine square window function in f2 dimension were applied before Fourier Transformation. ^{1}H,^{1}H-NOESY spectrum was acquired with 4096 data points in f2 and with 256 increments in f1, using 24 scans for each FID. The recycling delay was 3.5 s; pure phase line shapes were obtained by using time proportional phase incrementation (TPPI) phase cycling, mixing time of 1.7 s was used; one time zero filling in f1; π/2 shifted sine square window functions were applied to f2 and f1 dimensions before Fourier Transformation.

^{1}H DOSY NMR experiments were acquired in spin-off mode with the standard Bruker ledbpgp2s program using 16 or 32 t1 increments of 16 to 128 transients. The acquisition time was 2.0 s and the relaxation delay was 10 s (D1). Diffusion time was 0.3 s (D20) and rectangular gradient pulse duration was 0.6 ms (P30). Gradient recovery delays of 150 μs followed the application of each gradient pulse. Data were accumulated by linearly varying the diffusion encoding gradients over a range from 2 to 95 % for 16 or 32 gradient increment values. Processing of NMR data was performed using Topspin Program 3.1 and the diffusion coefficient was measured by T1/T2 relaxation module of the constructor's program (Bruker).

Mass Spectrometry. ESI-IMS-MS data were acquired on a Waters Synapt G2-S*i* mass spectrometer (Waters, UK) equipped with an Electrospray ionization source used in the positive ion mode. Infusion samples were prepared in acetonitrile containing 5.10^{-3} mg mL^{-1} of **2b** and **3**. For the mass spectrometer parameters, the Electrospray ionization (ESI) conditions were capillary voltage 3.1 kV; cone voltage 30 V; source temperature 100 °C; desolvation temperature 200 °C. Dry nitrogen, the desolvation gas, is used as the ESI gas with a flow rate

of 500 L h^{-1} for. For the HRMS (High Resolution Mass Spectrometry – Accurate Mass Measurements) measurements, a solution of NaI is used to prepare reference ions (lock masses). Ion mobility experiments were performed using the TWIMS cell constituting the so-called Tri-Wave setup, composed of three successive T-wave elements named the Trap cell, the IMS cell, and the Transfer cell, in which the wave speed and amplitude are user-tunable. The trap and transfer cells were filled with argon whereas the IMS cell was filled with nitrogen. A small rf-only cell filled with helium is fitted between the trap and the IMS cell. Signal attenuation (pDRE) down to 1% was used to limit ion diffusion in the traveling wave ion mobility cell, as a way to avoid IMS signals broadening. The IMS cell conditions were N_2 flow rate 80 mL min^{-1}, wave velocity 750 m s^{-1} and wave height 40 V. TWIMS data were analyzed using the Waters MassLynx SCN 901 software. Arrival time distributions (ATDs) were recorded by selecting the most abundant isotope for each ion composition to avoid unspecific selection. ATDs were converted into collisional cross-section (CCS) distributions in helium by means of a polymer calibration following a procedure detailed in the literature[60] using commercial PEG samples with average molecular weights of 600, 1000, 2000 and 3350 g mol^{-1} and PLA samples with average molecular weights of 4000, 5500 and 10 000 g mol^{-1}. The CCSs are determined at the APEX of the CCS distributions.

Molecular Dynamics Simulations of Gaseous Ions. Simulations of the gas phase behavior of **3** (14+) and **2b** (6+) were performed with Materials Studio 18.0[61] using the DREIDING[62] force field. The osmium atom was added with the same van der Waals parameters as for ruthenium. Gasteiger partial charges were used. A first quenched dynamics (NVT) was performed at 800 K for 25 ns, in vacuum. The most stable geometry among the 100 generated structures was reinjected in a second quenches dynamics (NVT) at 200K for 25 ns. The most stable structure was then used as a starting point for two consecutive MD simulations (NVT) at 298 K for 25 ns, in vacuum. 250 structures were extracted from the last MD simulation with 100 ps intervals, and further submitted to CCS calculations using the Trajectory Method as implemented in Collidoscope.[63]

UV−Visible Absorption. UV−vis absorption spectra were recorded on a Shimadzu UV-1700 with 1 cm path length quartz cell at 293 K.

Steady-State Photoluminescence. Fluorescence spectra were recorded on a FluoroLog3 FL3-22 from Jobin Yvon equipped with an 18 V, 450 W xenon short arc lamp and an R928P photomultiplier. Excitation and emission spectra are corrected for the instrument response. The PL quantum yield, Φ_{PL}, was measured by comparative actinometry using $[Ru(bpy)_3]^{2+}.2PF_6^-$ in acetonitrile[64] (Φ = 0.018) as a quantum yield standard for Ru(II)

compounds (excitation at 450 nm) and $[Os(bpy)_3](PF_6)_2$ in acetonitrile[56] ($\Phi = 0.005$) for Os(II) compound (excitation at 490 nm).

Time-Resolved Photoluminescence. Luminescence lifetimes measurements were performed after irradiation at λ = 400 nm obtained by the second harmonic of a titanium:sapphire laser (picosecond Tsunami laser spectra physics 3950-M1BB and 39868-03 pulse picker doubler) at a 0.8 MHz repetition rate. Fluotime 200 from AMS technologies was used for the decay acquisition. It consists of a GaAs microchannel plate photomultiplier tube (Hamamatsu model R3809U-50) followed by a time-correlated single-photon counting system from Picoquant (PicoHarp300). The ultimate time resolution of the system is close to 30 ps. Luminescence decays were analyzed with Fluofit software available from Picoquant.

Electrochemistry. Cyclic voltammetry (CV) and differential pulse voltammetry (DPV) was performed with an Autolab PGSTAT 100 potentiostat using a standard three-electrode-cell, *i.e.* a glassy carbon disk working electrode (approximate area = 0.03 cm^2), a platinum wire counter electrode and an aqueous Ag/AgCl reference electrode. Experiments were performed in dry 0.1 M $[nBu_4][PF_6]$ acetonitrile solution. Before each measurement, the solutions were purged by nitrogen. For cyclic voltammetry, a scan rate of 0.1 V/s was used. For differential pulse voltammetry an amplitude of 0.05 V, pulse width of 0.05 s, sample width of 0.0167 s and a pulse period of 0.2 s were used.

*$[Ru_3$**(L2a)**$(tpy)_3](PF_6)_6$* ***(2a)****:* To **L2a** (0.015 g, 0.0170 mmol, 1 equiv) and $[Ru(tpy)Cl_3]$ (0.0292 g, 0.0662 mmol, 3.9 equiv) was added a mixture of water/isopropanol/HFIP (14 mL, 4/3/1) and *N*-ethylmorpholine (0.5 mL). The reaction medium was heated to 90 °C in a microwave reactor for 2 hours and cooled down to room temperature. An excess of aqueous ammonium hexafluorophosphate was added to the solution and the resulting precipitate was collected and washed with water. The solid was purified by flash chromatography on SiO_2 (acetonitrile/saturated aqueous KNO_3/water:7/1/0.75). The desired fractions were concentrated and the product was precipitated by the addition of an excess of aqueous ammonium hexafluorophosphate. The precipitate was collected and washed three times with water to afford **2a** (0.0180 g, 39%) as a dark red solid.

^{1}H NMR (CD_3CN, 500 MHz): δ (ppm) 9.75-9.72 (m, 4H, H_c and H_d), 9.25 (s, 4H, $H_{3'}$ and $H_{5'}$), 8.93 (d, $J_{HB3'(HB5')\text{-}HB4'}$ = 8.4 Hz, 2H, $H_{B3'}$ and $H_{B5'}$), 8.80-8.76 (m, 8H, H_3, $H_{3''}$, $H_{A3'}$ and $H_{A5'}$), 8.66 (d, $J_{H3\text{-}H4}$ = 8.4 Hz, 2H, H_{B3} and $H_{B3''}$,), 8.57 (t, $J_{HB4'\text{-}\ HB3'(HB5')}$ = 8.4 Hz, 1H, $H_{B4'}$), 8.51-8.48 (m, 6H, H_{A3}, $H_{A3''}$ and H_e), 8.44 (t, $J_{HA4'\text{-}\ HA3'(HA5')}$ = 8.2 Hz, 2H, $H_{A4'}$), 8.06-8.03 (m, 4H, H_b, H_{B4} and $H_{B4''}$), 7.98-7.95 (m, 6H, H_f, H_4 and $H_{4''}$), 7.92 (t, $J_{HA4\text{-}\ HA3(HA5)}$ = 7.9 Hz, 4H, H_{A4} and $H_{A4''}$), 7.77 (d, $J_{Ha\text{-}\ Hb}$ = 5.7 Hz, 2H, H_a), 7.70 (d, $J_{HB6\text{-}\ HB5}$ = 5.6 Hz, 2H, H_{B6}

and $H_{B6''}$), 7.38 (d, $J_{H6(HA6)-H5(HA5)}$ = 5.4 Hz, 8H, H_6, $H_{6''}$, H_{A6} and $H_{A6''}$), 7.34-7.31 (m, 2H, H_{B5} and $H_{B5''}$), 7.21-7.19 (m, 4H, H_5 and $H_{5''}$), 7.15-7.13 (m, 4H, H_{A5} and $H_{A5''}$). HRMS (ESI): *m/z* calculated for $[C_{96}H_{65}N_{18}Ru_3]^{6+}$: 309.0332; found: 309.0337.

*[Ru$_3$(**L2b**)(tpy)$_3$](PF$_6$)$_6$ (**2b**):* To **2a** (0.0514 g, 0.0188 mmol, 1 equiv.), (4-([2,2':6',2''-terpyridin]-4'-yl)phenyl)boronic acid (0.0199 g, 0.0566 mmol, 3 equiv.) and K_2CO_3 (0.0391 g, 0.286 mmol, 15 equiv.) was added a mixture of *N*,*N*-dimethylformamide/water (7 mL, 2.5/1). The reaction mixture was degassed by four freeze-pump-thaw cycles. After the third cycle, when the reaction mixture was frozen, $[Pd(PPh_3)_4]$ (0.0020 g, 0.00283 mmol, 0.15 equiv.) was added and one more freeze-pump-thaw cycle was performed. The reaction mixture was heated at 85°C during 4h under argon and cooled down to room temperature. An excess of aqueous ammonium hexafluorophosphate was added to the solution and the resulting precipitate was collected and washed with water. The resulting precipitate was partially dissolved in 1 mL of tetrahydrofuran and re-precipitate by the addition of 15 ml of diethyl ether and collected by centrifugation. This was repeated until no residual precursor was detected in the supernatant by TLC on SiO_2. The precipitate was dried under vacuum, dissolved in acetonitrile and filtered through a 0.45 µm PTFE syringe filter. The resulting solution was dried to afford **2b** (0.0414 g, 74%) as a dark red solid.

^{1}H NMR (CD_3CN, 500 MHz): δ (ppm) 9.54 (s, 2H, H_d), 9.42 (d, J_{Hc-Hb} = 1.7 Hz, 2H, H_c), 9.06 (s, 4H, $H_{3'}$ and $H_{5'}$), 8.93 (d, $J_{HB3'(HB5')-HB4'}$ = 8.3 Hz, 2H, $H_{B3'}$ and $H_{B5'}$), 8.86 (s, 2H, H_i), 8.77 (d, $J_{HA3'(HA5')-HA4'}$ = 8.2 Hz, 4H, $H_{A3'}$ and $H_{A5'}$), 8.75-8.72 (m, 4H, H_m and H_j), 8.66 (d, $J_{H3(HB3)-H4(HB4)}$ = 8.1 Hz, 6H, $H_{3,}$ $H_{3''}$, H_{B3} and $H_{B3''}$), 8.61-8.56 (m, 3H, $H_{B4'}$ and H_e), 8.50 (d, $J_{HA3-HA4}$ = 8.0 Hz, 4H, H_{A3} and $H_{A3''}$), 8.45 (t, $J_{HA4'-HA3'(A5')}$ = 8.2 Hz, 2H, $H_{A4'}$), 8.21 (d, J_{Hf-He} = 8.5 Hz, 2H, H_f), 8.13 (d, J_{Hh-Hg} = 8.6 Hz, 2H, H_h or H_g), 8.10-8.08 (m, 2H, H_h or H_g), 8.08-8.05 (m, 2H, H_{B4} and $H_{B4''}$), 8.02-7.96 (m, 8H, H_b, H_k, H_4 and $H_{4''}$), 7.92 (td, $J_{HA4-HA3(A5)}$ = 8.0 Hz, $J_{HA4-HA6}$ = 1.4 Hz, 4H, H_{A4} and $H_{A4''}$), 7.79 (d, J_{Ha-Hb} = 5.8 Hz, 2H, H_a), 7.70 (d, $J_{HB6-HB5}$ = 5.8 Hz, 2H, H_{B6} and $H_{B6''}$), 7.47 (ddd, J_{Hl-Hm} = 4.7 Hz, J_{Hl-Hk} = 7.5 Hz, J_{Hl-Hj} = 1.2 Hz, 2H, H_l), 7.39 (dd, J_{H6-H5} = 5.5 Hz, J_{H6-H4} = 0.6 Hz, 4H, H_6 and $H_{6''}$), 7.35-7.33 (m, 6H, H_{A6}, $H_{A6''}$, H_{B5} and $H_{B5''}$), 7.23-7.21 (m, 4H, H_5 and $H_{5''}$), 7.16-7.13 (m, 4H, H_{A5} and $H_{A5''}$). HRMS (ESI): *m/z* calculated for $[C_{117}H_{79}N_{21}Ru_3]^{6+}$: 347.0669; found: 347.0678.

*[Os(Ru$_3$(**L2b**)(tpy)$_3$)$_2$](PF$_6$)$_{14}$ (**3**):* To **2b** (0.025 g, 0.00846 mmol, 2.66 equiv.) and K_2OsCl_6 (0.0015 g, 0.00317 mmol, 1 equiv.) was added ethylene glycol (4 mL) and *N*-ethylmorpholine (0.2 mL). The reaction medium was heated at 180 °C in a microwave reactor for 10 minutes and cooled down to room temperature. An excess of aqueous ammonium hexafluorophosphate was added to the solution and the resulting precipitate was collected and

washed with water. The solid was purified by a size exclusion chromatography on sephadex LH-20 (methanol/acetonitrile/water/saturated aqueous KNO_3:45/45/7.5/2.5). The desired fractions were concentrated and precipitated by the addition of an excess of aqueous ammonium hexafluorophosphate. The precipitate was collected and washed three times with water to afford $[Os(Ru_3(\mathbf{L2b})(tpy)_3)_2](PF_6)_{14}$ (0.0093 g, 46%) as a dark red solid.

^{1}H NMR (CD_3CN, 500 MHz): δ (ppm) 9.60 (s, 4H, H_d), 9.49 (d, $J_{Hc\text{-}Hb}$ = 1.4 Hz, 4H, H_c), 9.12 (s, 4H, H_i), 9.09 (s, 8H, $H_{3'}$ and $H_{5'}$), 8.94 (d, $J_{HB3'(HB5')\text{-}HB4'}$ = 8.3 Hz, 4H, $H_{B3'}$ and $H_{B5'}$), 8.77 (d, $J_{HA3'(HA5')\text{-}HA4'}$ = 8.2 Hz, 8H, $H_{A3'}$ and $H_{A5'}$), 8.69-8.58 (m, 20H, H_e, H_j, H_3, $H_{3''}$, H_{B3} and $H_{B3''}$), 8.60 (t, $J_{HB4'\text{-}HB3'(HB5')}$ = 8.3 Hz, 2H, $H_{B4'}$), 8.51 (d, $J_{HA3\text{-}HA4}$ = 8.0 Hz, 8H, H_{A3} and $H_{A3''}$), 8.45 (t, $J_{HA4'\text{-}HA3'(HA5')}$ = 8.2 Hz, 4H, $H_{A4'}$), 8.38 (d, $J_{Hh\text{-}Hg}$ = 8.4 Hz, 4H, H_h), 8.30 (d, $J_{Hf\text{-}He}$ = 8.4 Hz, 4H, H_f), 8.26 (d, $J_{Hg\text{-}Hh}$ = 8.4 Hz, 4H, H_g), 8.07 (td, $J_{HB4\text{-}HB3(HB5)}$ = 8.0 Hz, $J_{HB4\text{-}HB6}$ = 1.3 Hz, 4H, H_{B4} and $H_{B4''}$), 8.00-7.97 (m, 12H, H_4, $H_{4''}$ and H_b), 7.93 (td, $J_{HA4\text{-}HA3(HA5)}$ = 8.0 Hz, $J_{HA4\text{-}HA6}$ = 1.4 Hz, 8H, H_{A4} and $H_{A4''}$), 7.83 (td, $J_{Hk\text{-}Hj(Hl)}$ = 8.0 Hz, $J_{Hk\text{-}Hm}$ = 1.3 Hz, 4H, H_k), 7.80 (d, $J_{Ha\text{-}Hb}$ = 5.9 Hz, 4H, H_a), 7.73 (d, $J_{HB6\text{-}HB5}$ = 6.3 Hz, 4H, H_{B6} and $H_{B6''}$), 7.40-7.34 (m, 24H, H_m, H_6, $H_{6''}$, H_{A6}, $H_{A6''}$, H_{B5} and $H_{B5''}$), 7.23-7.21 (m, 8H, H_5 and $H_{5''}$), 7.17-7.14 (m, 12H, H_l, H_{A5} and $H_{A5''}$). HRMS (ESI): *m/z* calculated for $[C_{234}H_{158}N_{42}OsRu_6]^{14+}$: 311.0545; found: 311.0550.

ASSOCIATED CONTENT

Supporting Information

^{1}H NMR spectra, Mass spectrometry, Electrochemistry. The Supporting Information is available free of charge on the ACS Publications website.

AUTHOR INFORMATION

Corresponding Author

* Benjamin.elias@uclouvain.be

Author Contributions

The manuscript was written through contributions of all authors. All authors have given approval to the final version of the manuscript.

Funding Sources

Any funds used to support the research of the manuscript should be placed here (per journal style).

Notes

Any additional relevant notes should be placed here.

ACKNOWLEDGMENT

S. C. and B. E. gratefully acknowledge the UCLouvain for financial support. L. T.-G. is a postdoctoral researcher of the Fonds de la Recherche Scientifique – FNRS. The NanoBio-ICMG platform (FR 2607) is greatly acknowledged. The UMONS lab is grateful to the F.R.S.-FNRS for financial support in the acquisition of the Waters Synapt G2-Si mass spectrometer. QD is a FNRS research fellow.

References

1. Balzani, V.; Credi, A.; Venturi, M. In *Molecular Devices and Machines*; Wiley-VCH, Ed.; weinheim, 2008; Chapter 6, pp 135-169.
2. Balzani, V.; Bergamini, G.; Ceroni, P.; Marchi, E. Designing light harvesting antennas by luminescent dendrimers. *New J. Chem.* **2011**, *35*, 1944-1954.
3. Kavarnos, G. J.; Turro, N. J. Photosensitization by reversible electron transfer: theories, experimental evidence, and examples. *Chem. Rev.* **1986**, *86*, 401-449.
4. La Ganga, G.; Nastasi, F.; Campagna, S.; Puntoriero, F. Photoinduced water oxidation sensitized by a tetranuclear Ru(ii) dendrimer. *Dalton Trans.* **2009**, 9997-9999.
5. Natali, M.; Puntoriero, F.; Chiorboli, C.; La Ganga, G.; Sartorel, A.; Bonchio, M.; Campagna, S.; Scandola, F. Working the Other Way Around: Photocatalytic Water Oxidation Triggered by Reductive Quenching of the Photoexcited Chromophore. *J. Phys. Chem. C* **2015**, *119*, 2371-2379.
6. Puntoriero, F.; La Ganga, G.; Sartorel, A.; Carraro, M.; Scorrano, G.; Bonchio, M.; Campagna, S. Photo-induced water oxidation with tetra-nuclear ruthenium sensitizer and catalyst: A unique 4 × 4 ruthenium interplay triggering high efficiency with low-energy visible light. *Chem. Commun.* **2010**, *46*, 4725-4727.
7. Stoll, T.; Gennari, M.; Fortage, J.; Castillo, C. E.; Rebarz, M.; Sliwa, M.; Poizat, O.; Odobel, F.; Deronzier, A.; Collomb, M.-N. An Efficient RuII–RhIII–RuII Polypyridyl Photocatalyst for Visible-Light-Driven Hydrogen Production in Aqueous Solution. *Angew. Chem. Int. Ed.* **2014**, *53*, 1654-1658.
8. Cancelliere, A. M.; Puntoriero, F.; Serroni, S.; Campagna, S.; Tamaki, Y.; Saito, D.; Ishitani, O. Efficient trinuclear Ru(ii)–Re(i) supramolecular photocatalysts for CO2 reduction based on a new tris-chelating bridging ligand built around a central aromatic ring. *Chem. Sci.* **2020**, *11*, 1556-1563.
9. Li, F.; Jiang, Y.; Zhang, B.; Huang, F.; Gao, Y.; Sun, L. Towards A Solar Fuel Device: Light-Driven Water Oxidation Catalyzed by a Supramolecular Assembly. *Angew. Chem. Int. Ed.* **2012**, *51*, 2417-2420.
10. Elvington, M.; Brown, J.; Arachchige, S. M.; Brewer, K. J. Photocatalytic Hydrogen Production from Water Employing A Ru, Rh, Ru Molecular Device for Photoinitiated Electron Collection. *J. Am. Chem. Soc.* **2007**, *129*, 10644-10645.

11. Manbeck, G. F.; Fujita, E.; Brewer, K. J. Tetra- and Heptametallic Ru(II),Rh(III) Supramolecular Hydrogen Production Photocatalysts. *J. Am. Chem. Soc.* **2017**, *139*, 7843-7854.
12. Cerfontaine, S.; Wehlin, S. A. M.; Elias, B.; Troian-Gautier, L. Photostable Polynuclear Ruthenium(II) Photosensitizers Competent for Dehalogenation Photoredox Catalysis at 590 nm. *J. Am. Chem. Soc.* **2020**, *142*, 5549-5555.
13. Nomrowski, J.; Guo, X.; Wenger, O. S. Charge Accumulation and Multi-Electron Photoredox Chemistry with a Sensitizer–Catalyst–Sensitizer Triad. *Chem. Eur. J.* **2018**, *24*, 14084-14087.
14. Arrigo, A.; Puntoriero, F.; La Ganga, G.; Campagna, S.; Burian, M.; Bernstorff, S.; Amenitsch, H. Aggregation-Induced Energy Transfer in a Decanuclear Os(II)/Ru(II) Polypyridine Light-Harvesting Antenna Dendrimer. *Chem* **2017**, *3*, 494-508.
15. Puntoriero, F.; Serroni, S.; Nastasi, F.; Campagna, S. In *Electrochemistry of Functional Supramolecular Systems*; Wiley: 2010; Chapter 5, pp 121-143.
16. Campagna, S.; Denti, G.; Serroni, S.; Juris, A.; Venturi, M.; Ricevuto, V.; Balzani, V. Dendrimers of Nanometer Size Based on Metal Complexes: Luminescent and Redox-Active Polynuclear Metal Complexes Containing up to Twenty-Two Metal Centers. *Chem. Eur. J.* **1995**, *1*, 211-221.
17. Balzani, V.; Juris, A.; Venturi, M.; Campagna, S.; Serroni, S. Luminescent and Redox-Active Polynuclear Transition Metal Complexes. *Chem. Rev.* **1996**, *96*, 759-834.
18. Barigelletti, F.; Flamigni, L.; Balzani, V.; Collin, J.-P.; Sauvage, J.-P.; Sour, A.; Constable, E. C.; Thompson, A. M. W. C. Rigid Rod-Like Dinuclear Ru(II)/Os(II) Terpyridine-Type Complexes. Electrochemical Behavior, Absorption Spectra, Luminescence Properties, and Electronic Energy Transfer through Phenylene Bridges. *J. Am. Chem. Soc.* **1994**, *116*, 7692-7699.
19. Beley, M.; Chodorowski, S.; Collin, J.-P.; Sauvage, J.-P.; Flamigni, L.; Barigelletti, F. Luminescent Dinuclear Complexes Containing Ruthenium(II)- and Osmium(II)-Terpyridine-type Chromophores Bridged by a Rigid Biscyclometalating Ligand. *Inorg. Chem.* **1994**, *33*, 2543-2547.
20. Grosshenny, V.; Harriman, A.; Ziessel, R. Electronic Energy Transfer Across Ethynyl-Bridged RuII/OsII Terpyridyl Complexes. *Angewandte Chemie International Edition in English* **1995**, *34*, 1100-1102.
21. Barigelletti, F.; Flamigni, L.; Guardigli, M.; Juris, A.; Beley, M.; Chodorowski-Kimmes, S.; Collin, J.-P.; Sauvage, J.-P. Energy Transfer in Rigid Ru(II)/Os(II) Dinuclear Complexes with Biscyclometalating Bridging Ligands Containing a Variable Number of Phenylene Units. *Inorg. Chem.* **1996**, *35*, 136-142.
22. De Cola, L.; Belser, P. Photoinduced energy and electron transfer processes in rigidly bridged dinuclear Ru/Os complexes. *Coord. Chem. Rev.* **1998**, *177*, 301-346.
23. Faiz, J. A.; Williams, R. M.; Silva, M. J. J. P.; De Cola, L.; Pikramenou, Z. A Unidirectional Energy Transfer Cascade Process in a Ruthenium Junction Self-Assembled by α- and β-Cyclodextrins. *J. Am. Chem. Soc.* **2006**, *128*, 4520-4521.
24. Bilakhiya, A. K.; Tyagi, B.; Paul, P.; Natarajan, P. Di- and Tetranuclear Ruthenium(II) and/or Osmium(II) Complexes of Polypyridyl Ligands Bridged by a Fully Conjugated Aromatic Spacer: Synthesis, Characterization, and Electrochemical and Photophysical Studies. *Inorg. Chem.* **2002**, *41*, 3830-3842.

25. Campagna, S.; Denti, G.; Sabatino, L.; Serroni, S.; Ciano, M.; Balzani, V. A new hetero-tetrametallic complex of ruthenium and osmium: absorption spectrum, luminescence properties, and electrochemical behaviour. *J. Chem. Soc., Chem. Commun.* **1989**, 1500-1501.
26. La Mazza, E.; Puntoriero, F.; Nastasi, F.; Laramée-Milette, B.; Hanan, G. S.; Campagna, S. A heptanuclear light-harvesting metal-based antenna dendrimer with six Ru(ii)-based chromophores directly powering a single Os(ii)-based energy trap. *Dalton Trans.* **2016**, *45*, 19238-19241.
27. Larsen, J.; Puntoriero, F.; Pascher, T.; McClenaghan, N.; Campagna, S.; Åkesson, E.; Sundström, V. Extending the Light-Harvesting Properties of Transition-Metal Dendrimers. *ChemPhysChem* **2007**, *8*, 2643-2651.
28. Börje, A.; Köthe, O.; Juris, A. New luminescent and redox-active mono- and polynuclear ruthenium(ii) and osmium(ii) polypyridine complexes. *J. Chem. Soc., Dalton Trans.* **2002**, 843-848.
29. Denti, G.; Campagna, S.; Serroni, S.; Ciano, M.; Balzani, V. Decanuclear homo- and heterometallic polypyridine complexes: syntheses, absorption spectra, luminescence, electrochemical oxidation, and intercomponent energy transfer. *J. Am. Chem. Soc.* **1992**, *114*, 2944-2950.
30. Serroni, S.; Juris, A.; Venturi, M.; Campagna, S.; Resino, I. R.; Denti, G.; Credi, A.; Balzani, V. Polynuclear metal complexes of nanometre size. A versatile synthetic strategy leading to luminescent and redox-active dendrimers made of an osmium(II)-based core and ruthenium(II)-based units in the branches. *J. Mater. Chem.* **1997**, *7*, 1227-1236.
31. Predieri, G.; Vignali, C.; Denti, G.; Serroni, S. Characterization of merand fac isomers of [Ru(2,3-dpp)3][PF6]2 (2,3-dpp=2,3-bis(2-pyridyl)pyrazine) by 1H and 99Ru NMR spectroscopy. Proton assignment by 2D techniques. *Inorg. Chim. Acta.* **1993**, *205*, 145-148.
32. Bodige, S.; Torres, A. S.; Maloney, D. J.; Tate, D.; Kinsel, G. R.; Walker, A. K.; MacDonnell, F. M. First-Generation Chiral Metallodendrimers: Stereoselective Synthesis of Rigid D3-Symmetric Tetranuclear Ruthenium Complexes. *J. Am. Chem. Soc.* **1997**, *119*, 10364-10369.
33. Kim, M.-J.; MacDonnell, F. M.; Gimon-Kinsel, M. E.; Du Bois, T.; Asgharian, N.; Griener, J. C. Global Chirality in Rigid Decametallic Ruthenium Dendrimers. *Angew. Chem. Int. Ed.* **2000**, *39*, 615-619.
34. Campagna, S.; Serroni, S.; Bodige, S.; MacDonnell, F. M. Absorption Spectra, Photophysical Properties, and Redox Behavior of Stereochemically Pure Dendritic Ruthenium(II) Tetramers and Related Dinuclear and Mononuclear Complexes. *Inorg. Chem.* **1999**, *38*, 692-701.
35. Rutherford, T. J.; Van Gijte, O.; Kirsch-De Mesmaeker, A.; Keene, F. R. Stereoisomers of Mono-, Di-, and Triruthenium(II) Complexes Containing the Bridging Ligand 1,4,5,8,9,12-Hexaazatriphenylene and Studies of Their Photophysical Properties. *Inorg. Chem.* **1997**, *36*, 4465-4474.
36. Boice, G. N.; Garakyaraghi, S.; Patrick, B. O.; Sanz, C. A.; Castellano, F. N.; Hicks, R. G. Diastereomerically Differentiated Excited State Behavior in Ruthenium(II) Hexafluoroacetylacetonate Complexes of Diphenyl Thioindigo Diimine. *Inorg. Chem.* **2018**, *57*, 1386-1397.
37. Hiort, C.; Lincoln, P.; Norden, B. DNA binding of .DELTA.- and .LAMBDA.-[Ru(phen)2DPPZ]2+. *J. Am. Chem. Soc.* **1993**, *115*, 3448-3454.
38. Keane, P. M.; Poynton, F. E.; Hall, J. P.; Clark, I. P.; Sazanovich, I. V.; Towrie, M.; Gunnlaugsson, T.; Quinn, S. J.; Cardin, C. J.; Kelly, J. M. Enantiomeric Conformation Controls

Rate and Yield of Photoinduced Electron Transfer in DNA Sensitized by Ru(II) Dipyridophenazine Complexes. *J. Phys. Chem. Lett.* **2015**, *6*, 734-738.
39. Smith, J. A.; Collins, J. G.; Patterson, B. T.; Keene, F. R. Total enantioselectivity in the DNA binding of the dinuclear ruthenium(ii) complex [{Ru(Me2bpy)2}2(μ-bpm)]4+ {bpm = 2,2′-bipyrimidine; Me2bpy = 4,4′-dimethyl-2,2′-bipyridine}. *Dalton Trans.* **2004**, 1277-1283.
40. McDonnell, U.; Hicks, M. R.; Hannon, M. J.; Rodger, A. DNA binding and bending by dinuclear complexes comprising ruthenium polypyridyl centres linked by a bis(pyridylimine) ligand. *J. Inorg. Biochem.* **2008**, *102*, 2052-2059.
41. Niyazi, H.; Hall, J. P.; O'Sullivan, K.; Winter, G.; Sorensen, T.; Kelly, J. M.; Cardin, C. J. Crystal structures of Λ-[Ru(phen)2dppz]2+ with oligonucleotides containing TA/TA and AT/AT steps show two intercalation modes. *Nature Chem.* **2012**, *4*, 621-628.
42. McQuaid, K.; Abell, H.; Gurung, S. P.; Allan, D. R.; Winter, G.; Sorensen, T.; Cardin, D. J.; Brazier, J. A.; Cardin, C. J.; Hall, J. P. Structural Studies Reveal Enantiospecific Recognition of a DNA G-Quadruplex by a Ruthenium Polypyridyl Complex. *Angew. Chem. Int. Ed.* **2019**, *58*, 9881-9885.
43. Chakraborty, S.; Newkome, G. R. Terpyridine-based metallosupramolecular constructs: tailored monomers to precise 2D-motifs and 3D-metallocages. *Chem. Soc. Rev.* **2018**, *47*, 3991-4016.
44. Encinas, S.; Flamigni, L.; Barigelletti, F.; Constable, E. C.; Housecroft, C. E.; Schofield, E. R.; Figgemeier, E.; Fenske, D.; Neuburger, M.; Vos, J. G.; Zehnder, M. Electronic Energy Transfer and Collection in Luminescent Molecular Rods Containing Ruthenium(II) and Osmium(II) 2,2′:6′,2″-Terpyridine Complexes Linked by Thiophene-2,5-diyl Spacers. *Chem. Eur. J.* **2002**, *8*, 137-150.
45. Sauvage, J. P.; Collin, J. P.; Chambron, J. C.; Guillerez, S.; Coudret, C.; Balzani, V.; Barigelletti, F.; De Cola, L.; Flamigni, L. Ruthenium(II) and Osmium(II) Bis(terpyridine) Complexes in Covalently-Linked Multicomponent Systems: Synthesis, Electrochemical Behavior, Absorption Spectra, and Photochemical and Photophysical Properties. *Chem. Rev.* **1994**, *94*, 993-1019.
46. C. Constable, E. Metallodendrimers: metal ions as supramolecular glue. *Chem. Commun.* **1997**, 1073-1080.
47. Newkome, G. R.; Cardullo, F.; Constable, E. C.; Moorefield, C. N.; Thompson, A. M. W. C. Metallomicellanols: incorporation of ruthenium(II)–2,2′: 6′,2″-terpyridine triads into cascade polymers. *J. Chem. Soc. Chem. Comm.* **1993**, 925-927.
48. Constable, E. C.; Handel, R. W.; Housecroft, C. E.; Farràn Morales, A.; Ventura, B.; Flamigni, L.; Barigelletti, F. Metal-Directed Synthesis and Photophysical Studies of Trinuclear V-Shaped and Pentanuclear X-Shaped Ruthenium and Osmium Metallorods and Metallostars Based upon 4′-(3,5-Dihydroxyphenyl)-2,2′:6′,2′′-terpyridine Divergent Units. *Chem. Eur. J.* **2005**, *11*, 4024-4034.
49. Jacques, A.; Cerfontaine, S.; Elias, B. Access to Functionalized Luminescent Multi-2,2′:6′,2″-terpyridine Ligands. *J. Org. Chem.* **2015**, *80*, 11143-11148.
50. Cerfontaine, S.; Marcélis, L.; Laramee-Milette, B.; Hanan, G. S.; Loiseau, F.; De Winter, J.; Gerbaux, P.; Elias, B. Converging Energy Transfer in Polynuclear Ru(II) Multiterpyridine Complexes: Significant Enhancement of Luminescent Properties. *Inorg. Chem.* **2018**, *57*, 2639-2653.
51. Hilton, G. R.; Jackson, A. T.; Thalassinos, K.; Scrivens, J. H. Structural Analysis of Synthetic Polymer Mixtures Using Ion Mobility and Tandem Mass Spectrometry. *Anal. Chem.* **2008**, *80*, 9720-9725.

52. Benniston, A. C.; Harriman, A.; Li, P.; Sams, C. A. Comparison of the Photophysical Properties of Osmium(II) Bis(2,2‘:6‘,2‘ ‘-terpyridine) and the Corresponding Ethynylated Derivative. *J. Phys. Chem. A* **2005**, *109*, 2302-2309.
53. Wehlin, S. A. M.; Troian-Gautier, L.; Maurer, A. B.; Brennaman, M. K.; Meyer, G. J. Photophysical characterization of new osmium (II) photocatalysts for hydrohalic acid splitting. *J. Chem. Phys.* **2020**, *153*, 054307.
54. Sullivan, B. P.; Calvert, J. M.; Meyer, T. J. Cis-trans isomerism in (trpy)(PPh3)RuC12. Comparisons between the chemical and physical properties of a cis-trans isomeric pair. *Inorg. Chem.* **1980**, *19*, 1404-1407.
55. Takeko, M.-I.; Masahiro, T.; Takayoshi, M.; Tomoko, O. A Remarkably Rapid Synthesis of Ruthenium(II) Polypyridine Complexes by Microwave Irradiation. *Chem. Lett.* **1994**, *23*, 2443-2446.
56. Kober, E. M.; Caspar, J. V.; Lumpkin, R. S.; Meyer, T. J. Application of the energy gap law to excited-state decay of osmium(II)-polypyridine complexes: calculation of relative nonradiative decay rates from emission spectral profiles. *J. Phys. Chem.* **1986**, *90*, 3722-3734.
57. Four, P.; Guibe, F. Palladium-catalyzed reaction of tributyltin hydride with acyl chlorides. A mild, selective, and general route to aldehydes. *J. Org. Chem.* **1981**, *46*, 4439-4445.
58. Cave, G. W. V.; Raston, C. L. Efficient synthesis of pyridines via a sequential solventless aldol condensation and Michael addition. *J. Chem. Soc., Perkin Trans. 1* **2001**, 3258-3264.
59. Xie, T. Z.; Liao, S. Y.; Guo, K.; Lu, X.; Dong, X.; Huang, M.; Moorefield, C. N.; Cheng, S. Z.; Liu, X.; Wesdemiotis, C.; Newkome, G. R. Construction of a highly symmetric nanosphere via a one-pot reaction of a tristerpyridine ligand with Ru(II). *J. Am. Chem. Soc.* **2014**, *136*, 8165-8.
60. Duez, Q.; Chirot, F.; Liénard, R.; Josse, T.; Choi, C.; Coulembier, O.; Dugourd, P.; Cornil, J.; Gerbaux, P.; De Winter, J. Polymers for Traveling Wave Ion Mobility Spectrometry Calibration. *J. Am. Soc. Mass. Spectrom.* **2017**, *28*, 2483-2491.
61. Dassault Systèmes BIOVIA, Materials Studio, 18.0, Dassault Systèmes, San Diego, 2018
62. Mayo, S. L.; Olafson, B. D.; Goddard, W. A. DREIDING: a generic force field for molecular simulations. *J. Phys. Chem.* **1990**, *94*, 8897-8909.
63. Ewing, S. A.; Donor, M. T.; Wilson, J. W.; Prell, J. S. Collidoscope: An Improved Tool for Computing Collisional Cross-Sections with the Trajectory Method. *J. Am. Soc. Mass. Spectrom.* **2017**, *28*, 587-596.
64. Suzuki, K.; Kobayashi, A.; Kaneko, S.; Takehira, K.; Yoshihara, T.; Ishida, H.; Shiina, Y.; Oishi, S.; Tobita, S. Reevaluation of absolute luminescence quantum yields of standard solutions using a spectrometer with an integrating sphere and a back-thinned CCD detector. *PCCP* **2009**, *11*, 9850-9860.

For TOC use only

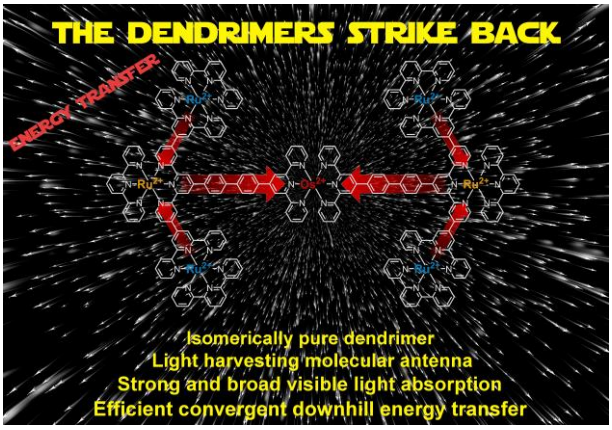

A novel stereoisomerically pure heptanuclear Ru(II)-Os(II) dendrimer is reported. This dendrimer exhibits large molar absorption coefficient (ε = 77,900 $M^{-1}cm^{-1}$ at 497 nm). Visible light excitation leads to unitary downhill energy transfer from the peripheral Ru(II) subunits to the Os(II) center that displays photoluminescence with a lifetime (τ =161ns) competent for diffusional excited-state electron transfer reactivity in solution.